Open access • Journal Article • DOI:10.1364/AO.21.000021

Photothermal spectroscopy of scattering media — Source link

Zafer A. Yasa, Warren B. Jackson, Nabil M. Amer

Institutions: Lawrence Berkeley National Laboratory

Published on: 01 Jan 1982 - Applied Optics (Optical Society of America)

Topics: Photothermal spectroscopy, Photothermal microspectroscopy, Photothermal therapy, Scattering and Photoacoustic spectroscopy

Title
PHOTOTHERMAL SPECTROSCOPY OF SCATTERING MEDIA

Authors
Yasa, Z.A.
Jackson, W.B.
Amer, N.M.

Publication Date
1981-08-01

LBL-13275
Preprint

Lawrence Berkeley Laboratory
UNIVERSITY OF CALIFORNIA

ENERGY & ENVIRONMENT
DIVISION

Submitted to Applied Optics

PHOTOTHERMAL SPECTROSCOPY OF SCATTERING MEDIA

Zafer A. Yasa, Warren B. Jackson, and Nabil M. Amer

August 1981

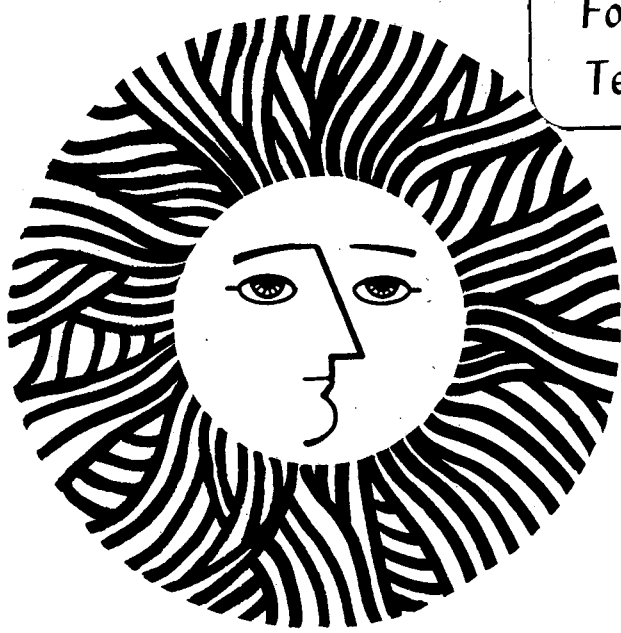

Prepared for the U.S. Department of Energy under Contract W-7405-ENG-48

PHOTOTHERMAL SPECTROSCOPY OF SCATTERING MEDIA

Zafer A. Yasa, Warren B. Jackson,[a] and Nabil M. Amer

Applied Physics and Laser Spectroscopy Group
Lawrence Berkeley Laboratory
University of California
Berkeley, California 94720

This work was supported by the Office of Energy Research, Pollution Characterization and Measurement Division of the U.S. Department of Energy under Contract No. W-7405-ENG-48.

PHOTOTHERMAL SPECTROSCOPY OF SCATTERING MEDIA

Zafer A. Yasa, Warren B. Jackson,[(a)] and Nabil M. Amer

Applied Physics and Laser Spectroscopy Group

Lawrence Berkeley Laboratory

University of California

Berkeley, California 94720

ABSTRACT

We present a general, unified theoretical analysis of the role of scattering in photothermal spectroscopy. We show that while the photothermal signal is significantly affected in the case of highly scattering media, it is independent of scattering for optically thin samples. Numerical estimates of the scattering contribution and comparison with experimental results are given. We also elucidate the relationship between photothermal and diffuse reflectance spectroscopies.

PHOTOTHERMAL SPECTROSCOPY OF SCATTERING MEDIA

Zafer A. Yasa, Warren B. Jackson,[(a)] and Nabil M. Amer

Applied Physics and Laser Spectroscopy Group

Lawrence Berkeley Laboratory

University of California

Berkeley, California 94720

Introduction

Insensitivity to scattering has generally been assumed to be an inherent characteristic of photoacoustic spectroscopy[1] since the photoacoustic signal is proportional to the fraction of energy absorbed which is converted to heat. Consequently, even for a highly scattering medium, the photoacoustic signal is presumed to be a direct measure of its absorption cross-section. However, it is well known that the reflectance of such a medium, which is conventionally studied by diffuse reflectance spectroscopy, is a complicated function of its scattering properties[2,3] as well as its absorption. The total absorbed energy, while proportional to the absorption cross-section, α_a, is also a function of the intensity distribution in the sample, which can deviate significantly from Beer's law when multiple scattering is important. Therefore, in principle, the thermal signal generated is affected by scattering. This has first been discussed by Helander *et al.*[4], who considered the special case of a semi-infinite (optically and thermally

thick) and isotropically scattering sample.

In this paper, we present a general unified analysis of the effects of light scattering in most common photothermal (photoacoustic and photothermal deflection[5]) spectroscopies (PTS) for arbitrary sample thicknesses and scattering characteristics. By simultaneously analyzing the heat diffusion equation and the radiative transport equation, we determine the photothermal signal, S, in terms of the optical and thermoelastic constants of the sample. We thereby rigorously establish the relationship between (1) photothermal spectroscopies and (2) optical transmission and reflectance spectroscopies. We show that, in general, PTS is significantly affected by strong scattering.

For low modulation frequencies such that $\ell_{th} >> \ell$ or $\ell_{th} >> \ell_{op}$, where ℓ, ℓ_{th}, and ℓ_{op} are the sample, thermal, and optical lengths , respectively, (i.e., when energy is deposited in a distance much shorter than the thermal length), we determine <u>exactly</u> that $S \propto [1-(R+T)]$ where R(T) is the diffuse and specular reflectance (transmittance) of the sample. For an optically thick sample (T=0), this expression implies that $S \propto (1-R)$ and, therefore, that the photothermal spectrum of a sample is in principle equivalent to its diffuse reflectance spectrum in this limit. As the modulation frequency is increased, we show that S varies from $S \propto [1-(R+T)]$ to $S \propto \alpha_a [1+2R(1+r_o)/(1-r_o)]$ (where r_o is the sample surface reflectance for internally incident diffuse light), depending on the optical properties (scattering, absorption) and the thermal diffusivity of the sample. This variation of S occurs because of the dependence of the heat flow on modulation frequency. Hence, we stress that PTS can yield important information unavailable by optical methods which, com-

bined with optical measurements, can be very useful for the determination of the optical constants of highly scattering media.

Using the above results, we also show that, for optically thin media, S is independent of scattering when $\alpha_s \ell \leq 0.1$ (α_s = scattering coefficient). This independence is in significant contrast to an optical measurement which would be dominated by scattering if $\alpha_s \ell \geq \alpha_a \ell$.

In Section II, we derive the general expression for S for the most commonly encountered cw PTS experimental configurations. In general, the PTS signal is given by a weighted average of the sample temperature distribution, which we determine in terms of an arbitrary intensity distribution in Section II(A). In Section II(B), utilizing the equation of radiative transfer for diffuse photons, we solve for the integrals of the sample intensity distribution which appear in the temperature solutions. In Section II(C), we determine the low frequency, high frequency, and semi-infinite sample limits. The results in Sections II(A-C) involve the measurable (external) optical properties of the sample R and T. These can be determined in terms of the intrinsic optical parameters (e.g. α_a , α_s) from the equation of radiative transfer by approximate analytical methods or numerically. The approximate expressions for R and T using a 3-flux calculation are given in Section II(D), and S is evaluated in the limits of Section II(C).

In Section III, we evaluate our theoretical results for some special cases, and compare our theoretical findings with the experimental measurements of Helander et al.[4] We discuss the implications of our results for the photothermal spectroscopy of highly scattering media.

II. Theory

A. General Solution for the Photothermal Signal in Terms of the Photon Distribution in the Sample

We consider media with isotropic and homogeneous thermoelastic and optical properties but which may be porous (see Table I). Porous media are taken into account by effective values of these properties[6,7] which may also be complex and frequency dependent (see Table II). We neglect fluorescence, thermal radiation, energy migration etc.

The signal, S, generated in the most common cw photothermal experiments can be written as[5,8-10]

$$S(\omega) = T_e(\omega) \iiint_{V_s} G(\vec{r})\tau(\vec{r})d^3\vec{r}$$

where $T_e(\omega) = T_r(\omega)T_t(\omega)$, $T_t(\omega)$ is a thermoelastic transduction factor, $T_r(\omega)$ is the transducer response (including a possible Helmholtz resonance response), $\tau(\vec{r})$ is the temperature distribution in the sample, V_s is the sample volume, and ω is the frequency. $G(\vec{r})$ is a geometrical weighting factor describing the relative contributions of the sample temperature distribution in the thermoacoustic conversion. In Table I, the expressions for $T_e(\omega)$ and $G(\vec{r})$ are given for the four major groups of cw PTS configurations (see Fig. 1), and the various material parameters are defined.

In the case of resonant fluid-transducer (FT) detection, we consider cylindrically symmetric, zero order longitudinal and low order radial modes, for which the laterally diffused beam diameter is much smaller than the mode diameter. Hence, $G(\vec{r}) \rightarrow 1$. (This assumption may

not be valid for high order modes excited by large diameter beams in highly scattering fluids). Thus, FT detection (resonant and nonresonant) is a special case of sample-fluid-transducer (SFT) detection with a fluid sample completely filling the cell.

Photothermal deflection spectroscopy (PDS) is also a special case of SFT detection. The equation in Table I for PDS has a somewhat restricted validity. When the scattering length is much less than the beam diameter, this equation is exact. Using the photon diffusion equation or intuitive arguments, we find that, when the scattering length is much larger than the beam diameter, the scattering contribution to the PDS signal is reduced by the scattering length divided by the beam diameter when compared to the scattering contribution to SFT.

Cw solid-transducer (ST) detection is not widely applicable to highly scattering media due to scattered light incident directly on the transducer. However, for completeness, we derive the fundamental equations pertaining to this technique in the Appendix.

Since the SFT case is general, we write

$$S(\omega) = T_e(\omega)\left[\frac{1}{k_f}\,\bar{\tau}(0) + \frac{\beta_s}{\beta_f}\,\chi\int_0^{\ell}\bar{\tau}(z)\,dz\right] \tag{1}$$

where $\bar{\tau}(z) \equiv \iint_S \tau(\vec{r})\,d^2\vec{\rho}$ is the average sample temperature in the transverse plane at z. The first term in the brackets in Eq. (1) gives the signal contribution due to the heat diffusion from the sample into the fluid. The form $\bar{\tau}(0)$ implies that only the energy deposited near (within a thermal length) the surface contributes to the signal. How-

ever, the contribution of the second term, which is due to the thermal expansion of the sample, depends on all the energy deposited in the sample. We assume that the contribution due to the buckling of a solid sample is negligible. For FT detection, only the second term contributes with X=1 and for PDS only the first term contributes.

In Figure 2, the sample geometry is sketched. We have assumed that the incident beam size << transverse sample dimensions and that the media on either side of the sample are thermally thick. We have also assumed that the cell boundaries are perfectly rigid and that the pressure within the sample equalizes with the pressure in the fluid. For porous media this condition may be violated since the sample may be larger than the pressure diffusion length.[6]

Integrating the heat equation over the transverse plane in the sample, and using the condition that no heat flux reaches the sample sides, the average temperature at plane z in the sample (oscillating at frequency ω) satisfies

$$\left(\frac{d^2}{dz^2} - k^2\right) \bar{\tau}(z) = -\frac{\alpha_a}{\kappa} P(z) \tag{2}$$

with the boundary conditions

$$\kappa \frac{d\bar{\tau}}{dz}\bigg|_{z=0} = \kappa_f k_f \bar{\tau}(0) \quad , \quad \kappa \frac{d\bar{\tau}}{dz}\bigg|_{z=\ell} = -\kappa_b k_b \bar{\tau}(\ell) \tag{2a}$$

$P(z) = \iint_S I(\vec{r})\, d^2\vec{\rho}$ is the power distribution in the sample (oscillating at frequency ω), $k^2 = i\omega\rho C_p/\kappa$, $k_f^2 = i\omega\rho_f C_f/\kappa_f$, $k_b^2 = i\omega\rho_b C_b/\kappa_b$, and $\kappa, \kappa_f, \kappa_b$ = thermal conductivity and $\rho C_p, \rho_f C_f, \rho_b C_b$ = heat capacity/unit volume at constant pressure of the sample, fluid and backing, respectively.

The general solution of Eq. (2) subject to Eq. (2a) is

$$\bar{\tau}(z) = \frac{\alpha_a}{2\kappa k}\left\{C_0[(1+g)e^{kz}+(1-g)e^{-kz}] + e^{-kz}\int_0^z P(\zeta)e^{k\zeta}d\zeta - e^{kz}\int_0^z P(\zeta)e^{-k\zeta}d\zeta\right\} \tag{3}$$

where

$$C_0 = \frac{[(1-b)e^{-k\ell}\int_0^\ell P(z)e^{kz}dz + (1+b)e^{k\ell}\int_0^\ell P(z)e^{-kz}dz]}{[(1+b)(1+g)e^{k\ell} - (1-b)(1-g)e^{-k\ell}]} \tag{3a}$$

and $g \equiv \frac{\kappa_f k_f}{\kappa k}$, $b \equiv \frac{\kappa_b k_b}{\kappa k}$.

Integrating Eq. (2) over $0 \le z \le \ell$ and using Eq. (2a), we find

$$\int_0^\ell \bar{\tau}(z)dz = \frac{1}{\kappa k^2}\left[\alpha_a\int_0^\ell P(z)dz - \kappa_b k_b\bar{\tau}(\ell) - \kappa_f k_f\bar{\tau}(0)\right] \tag{4}$$

in which, from Eqs. (3) and (3a)

$$\bar{\tau}(0) = \frac{\alpha_a\,[(1-b)e^{-k\ell}\int_0^\ell P(z)e^{kz}\,dz + (1+b)e^{k\ell}\int_0^\ell P(z)e^{-kz}dz]}{\kappa k\,[(1+b)(1+g)e^{k\ell} - (1-b)(1-g)e^{-k\ell}]} \tag{5}$$

$$\bar{\tau}(\ell) = \frac{\alpha_a\,[(1+g)\int_0^\ell P(z)e^{kz}dz + (1-g)\int_0^\ell P(z)e^{-kz}dz]}{\kappa k\,[(1+b)(1+g)e^{k\ell} - (1-b)(1-g)e^{-k\ell}]} \tag{6}$$

The terms in Eq. (4) have a simple physical interpretation. The first term is the total energy/sec deposited in the sample. The second and third terms are the heat flux/sec out of the back and front surfaces of the sample, respectively. Hence, the terms within the brackets give the net energy increase/sec of the sample. The multiplication factor converts the energy increase/sec into a temperature rise/cycle.

Eqs. (4), (5), and (6) substituted into Eq. (1) yield the photothermal signal in terms of weighted averages of the optical power distribution in the sample of the form $\int_0^\ell P(z)\exp(\pm kz)\,dz$. In the next section, these integrals are determined for a sample which has both absorption and scattering.

B. Solution for $\int_0^\ell P(z)\exp(kz)\,dz$

Assuming that a collimated beam of power, P_o, incident on the sample at z=0, the optical power distribution in the sample, P(z), is the sum of diffuse and collimated components

$$P(z) = \int_{-1}^{1} P_d(z,\mu)d\mu + P_0 \exp(-\alpha z) \tag{7}$$

where $P_d(z,\mu)$ is the diffuse power (diffuse intensity distribution integrated over the transverse plane) at z, propagating at an angle θ ($\mu=\cos\theta$) relative to the z-direction (Fig. 3). The collimated beam decays by the total attenuation coefficient $\alpha = \alpha_a + \alpha_s$.

Assuming macroscopically homogeneous and isotropic media, assuming incoherent and elastic scattering, and neglecting depolarization effects, the diffuse power distribution satisfies[11-13]

$$\mu \frac{d}{dz} P_d(z,\mu) = -\alpha P_d(z,\mu) + \alpha_s \int_{-1}^{1} s(\mu,\mu')P_d(z,\mu')d\mu' + \alpha_s P_0 \exp(-\alpha z)s(\mu,1) \tag{8}$$

where $s(\mu,\mu') \equiv s(\theta-\theta')$ is the indicatrix of anisotropic scattering describing the angular distribution of scattered photons (relative amount scattered from the cone θ to θ'). $s(\mu,\mu')$ is symmetric

$(s(\mu,\mu') = s(\mu',\mu))$ and normalized $(\int_{-1}^{1} s(\mu,\hat{\mu})\, d\mu = \int_{-1}^{1} s(\mu,\mu')d\mu' = 1)$. It is a function of the diameter, d, relative to wavelength, λ, and of the shape of the refractive index inhomogeneities; it is specified as a mean over a distribution of sizes and shapes. For isotropic scattering $s(\mu,\mu')=1/2$. For $\lambda/d \lesssim 1$ (Mie scattering) $s(\mu,\mu')$ is elongated in the forward direction ($\mu=\mu'$). For $\lambda/d >> 1$ (Rayleigh scattering) $s(\mu,\mu') = [\cos^2(\theta-\theta')+1]3/8$.

Eq. (8) is the radiative transfer equation describing the energy balance for the net change of $P_d(z,\mu)$ per unit length in the propagation direction. It states that the diffuse light $P_d(z,\mu)$ at z propagating in the μ direction is decreased by absorption and scattering (first term), increased by the diffuse light scattered in the μ direction from the diffuse photons propagating in all other directions (second term) and increased by photons scattered diffusely into the μ direction from the collimated beam propagating in the $\mu=1$ direction (third term). For simplicity, we have neglected the specular reflections of the collimated beam at the boundaries. These reflections, which are generally small, can be taken into account by a simple modification of the last term in Eq. (8). The boundary conditions for diffuse light are to be taken into account by defining the relevant reflection coefficients at the boundaries.

It is not possible to obtain exact analytical solutions of Eq. (8) for arbitrary $s(\mu,\mu')$ and sample length. A simplification follows, however, since only integrals of the form $\int_0^{\ell} P(z)\exp(\pm kz)dz$ are needed for the determination of S from Eqs. (1) and (4-6). We multiply Eq. (8) by $\exp(kz)$ and integrate over $0 \leq z \leq \ell$ obtaining

$$\mu[P_d(\ell,\mu)\exp(k\ell) - P_d(0,\mu)] = (k\mu-\alpha)\,\hat{P}_d(k,\mu) + \alpha_s \int_{-1}^{1} \hat{P}_d(k,\mu')s(\mu,\mu')d\mu'$$

$$+ \frac{\alpha_s}{(\alpha-k)} P_0\,(1-\exp(-\alpha+k)\ell)\; s(\mu,1)$$

where

$$\hat{P}_d(k,\mu) \equiv \int_0^{\ell} P_d(z,\mu)\exp(kz)dz \quad .$$

Defining

$$\hat{P}_d^{+} = \int_0^{1} \hat{P}_d(k,\mu)d\mu$$

$$\hat{P}_d^{-} = \int_{-1}^{0} \hat{P}_d(k,\mu)\; d\mu$$

$$\Phi^{+}(x) = \int_0^{1} P_d(x,\mu)\mu d\mu \qquad (9)$$

$$\Phi^{-}(x) = -\int_{-1}^{0} P_d(x,\mu)\mu d\mu$$

and adding and subtracting the integrals of the above equation over $0 \le \mu \le 1$ and $-1 \ge \mu \ge 0$, we obtain

$$[\Phi^{+}(\ell)\exp(k\ell)-\Phi^{+}(0)] - [\Phi^{-}(\ell)\exp(k\ell)-\Phi^{-}(0)]$$

$$= k\left[\int_0^{1} \mu\hat{P}(k,\mu)d\mu + \int_{-1}^{0} \mu\hat{P}(k,\mu)d\mu\right] - \alpha_a(\hat{P}_d^{+}+\hat{P}_d^{-}) + \frac{\alpha_s}{(\alpha-k)} P_0[1-\exp(-\alpha+k)\ell]$$

$$[\Phi^+(\ell)\exp(k\ell)-\Phi^+(0)] + [\Phi^-(\ell)\exp(k\ell)-\Phi^-(0)]$$

$$= k\left[\int_0^1 \mu\hat{P}_d(k,\mu)d\mu - \int_{-1}^0 \mu\hat{P}_d(k,\mu)d\mu\right] - \alpha(\hat{P}_d^+-\hat{P}_d^-)$$

$$+ \alpha_s \int_{-1}^1 \hat{P}_d(k,\mu')\left[\int_0^1 s(\mu,\mu')d\mu - \int_{-1}^0 s(\mu,\mu')d\mu\right]d\mu'$$

$$+ \frac{\alpha_s}{(\alpha-k)}\,\eta\,P_0\,[1 - \exp(-\alpha+k)\ell]$$

where $\eta \equiv 1 - 2\int_{-1}^0 s(\mu,1)d\mu$ (10)

Then we apply the Schuster-Schwarzchild (Kubelka-Munk) approximation commonly used in radiative transfer theory[12] by setting

$$\int_0^1 \mu\hat{P}_d(k,\mu)d\mu = \frac{1}{2}\hat{P}_d^+$$

$$\int_{-1}^0 \mu\hat{P}_d(k,\mu)d\mu = -\frac{1}{2}\hat{P}_d^-$$

$$\int_0^1 \hat{P}_d(k,\mu')\int_{-1}^0 s(\mu,\mu')d\mu d\mu' = \frac{\Lambda}{2}\hat{P}_d^+ \qquad (11)$$

$$\int_{-1}^0 \hat{P}_d(k,\mu')\int_0^1 s(\mu,\mu')d\mu d\mu' = \frac{\Lambda}{2}\hat{P}_d^-$$

Note that Λ and η are parameters that take in account the anisotropy of scattering. Λ describes the ratio of the backscattered to the forward scattered diffuse photons and η describes the difference between the relative number of photons diffusely scattered from the collimated beam into the forward and backward directions. In general, $0 \leq \eta \leq 1$, $0 \leq \Lambda \leq 1$ and $\Lambda = 1, \eta = 0$ for isotropic scattering. Eq. (11) becomes exact if the diffuse light is uniformly distributed in each of the forward and backward hemispheres. Using Eq. (11), we obtain

$$[\Phi^+(\ell)\exp(k\ell)-\Phi^+(0)] - [\Phi^-(\ell)\exp(k\ell)-\Phi^-(0)] = \frac{k}{2}(\hat{P}_d^+-\hat{P}_d^-) - \alpha_a(\hat{P}_d^++\hat{P}_d^-) + \frac{\alpha_s}{(\alpha-k)} P_0 [1-\exp(-\alpha+k)\ell]$$

$$[\Phi^+(\ell)\exp(k\ell)-\Phi^+(0)] + [\Phi^-(\ell)\exp(k\ell)-\Phi^-(0)] = \frac{k}{2}(\hat{P}_d^++\hat{P}_d^-) - (\alpha_a+\alpha_s\Lambda)(\hat{P}_d^+-\hat{P}_d^-) + \frac{\alpha_s}{(\alpha-k)} \eta P_0 [1-\exp(-\alpha+k)\ell]$$

which can be solved simultaneously for $\hat{P}_d^+ + \hat{P}_d^-$, giving the result

$$\int_0^\ell P(z)\exp(kz)dz = \hat{P}_d^+ + \hat{P}_d^- + \frac{P_0}{(\alpha-k)}\left[1-\exp(-\alpha+k)\ell\right]$$

$$= \left[k^2-4\alpha_a(\alpha_a+\alpha_s\Lambda)\right]^{-1}\left\{2\left[\kappa+2(\alpha_a+\alpha_s\Lambda)\right]\left[\Phi^+(\ell)\exp(k\ell)-\Phi^+(0)\right]\right.$$

$$+ 2\left[k-(\alpha_a+\alpha_s\Lambda)\right]\left[\Phi^-(\ell)\exp(k\ell)-\Phi^-(0)\right]$$

$$\left.+ \frac{P_0}{(\alpha-k)}\left[k^2-4\alpha(\alpha_a+\alpha_s\Lambda)-2n\alpha_s k\right]\left[1-\exp(-\alpha+k)\ell\right]\right\} \tag{12}$$

In Eq. (12), the fluxes at the boundaries $\Phi^{\pm}(0)$ and $\Phi^{\pm}(\ell)$ can be written in terms of the total reflected and transmitted fluxes from the sample using the boundary conditions

$$\Phi^+(0) = r_0\Phi^-(0)$$

$$\Phi^-(\ell) = r_\ell\Phi^+(\ell) + r_{c\ell}P_0\exp(-\alpha\ell) \tag{13}$$

and definitions

$$\Phi^-(0) - \Phi^+(0) \equiv RP_0$$

$$\Phi^+(\ell) - \Phi^-(\ell) + P_0\exp(-\alpha\ell) \equiv TP_0 \tag{14}$$

In Eqs. (13) and (14), r_o and r_ℓ are the effective reflection coefficients for internally incident diffuse light at the sample boundaries, $r_{c\ell}$ is the coefficient for diffuse reflection of the collimated flux at $z=\ell$, and R and T are the reflectance and transmittance of the sample, respectively. Due to total internal reflection for incidence angles greater than the critical angle, r_o and r_ℓ have values substantially higher than for normal incidence. (For isotropically diffuse light $r_{o,\ell} \approx 0.6$ for a refractive index ratio of 1.5.) In some experiments, the backing medium may be a high diffuse reflector[14] for which r_ℓ and $r_{c\ell}$ assume values close to unity.

Substituting Eqs. (13) and (14) into Eq. (12), we obtain

$$\int_0^\ell P(z)\exp(kz)dz = \frac{P_0}{[k^2-4\alpha_a(\alpha_a+\alpha_s\Lambda)]} \left\{ 2R\left[2(\alpha_a+\alpha_s\Lambda)-k\left(\frac{1+r_0}{1-r_0}\right)\right] + 2Te^{k\ell}\left[2(\alpha_a+\alpha_s\Lambda) + k\left(\frac{1+r_\ell}{1-r_\ell}\right)\right] + \frac{[k^2-4\alpha(\alpha_a+\alpha_s\Lambda)-2n\alpha_s k]}{(\alpha-k)} + \frac{ke^{(-\alpha+k)\ell}}{(\alpha-k)}\left[k+2\alpha_a+2\alpha_s(2\Lambda+n-1) + 4(\alpha-k)\frac{r_{c\ell}}{1-r_\ell}\right]\right\} \quad (15)$$

For isotropic scattering ($\Lambda=1$, $\eta=0$) and $r_{c\ell}=0$, Eq. (15) reduces to

$$\int_0^{\ell} P(z)\exp(kz)dz = \frac{P_0}{(k^2-4\alpha_a\alpha)} \left\{2R\left[2\alpha-k\left(\frac{1+r_0}{1-r_0}\right)\right] + 2Te^{k\ell}\left[2\alpha+k\left(\frac{1+r_\ell}{1-r_\ell}\right)\right] - \frac{2\alpha+k}{(\alpha-k)}\left[2\alpha-k(1+\exp(-\alpha+k)\ell\right]\right\} \tag{15a}$$

C. Special Cases

Eq. (15) substituted into Eqs. (1) and (4-6) yields the photothermal signal in terms of the modulation frequency and the optical properties of the sample. Of particular interest are the limiting cases as $\omega\to 0$, $\omega\to\infty$, and $\ell\to\infty$ which are treated in this section.

1. $\ell_{th}\equiv 1/|k| \gg \ell$ or $\ell_{th} \gg \ell_{op}\equiv 1/\alpha$

This is the case when the energy is deposited in a region much shorter than the thermal length (see Fig. 4). We can set $\int_0^{\ell} P(z)\exp(kz)dz \simeq \int_0^{\ell} P(z)dz$ which, by direct integration of Eq. (8) and using Eq. (4), is given by

$$\alpha_a \int_0^{\ell} P(z)dz = [1-(R+T)]\, P_0 \tag{16}$$

Using the above in Eqs. (1) and (4-6) implies that in this limit

$$S \longrightarrow T_e(\omega)\, \frac{P_0}{\kappa k k_f}\, F(\omega)[1-(R+T)] \tag{17}$$

where

$$F(\omega) = \frac{[(1-b)\exp(-k\ell)+(1+b)\exp(k\ell)]\ [1 + \frac{\beta_s}{\beta_f} \chi \frac{k_f}{k}] - \frac{2b\beta_s}{\beta_f} \chi \frac{k_f}{k}}{[(1+b)(1+g)\exp(k\ell) - (1-b)(1-g)\exp(k\ell)]}$$

Note that in this limit, Eq. (17) is independent of the Schuster-Schwarzchild approximation (Eq. (11)) introduced for the general solution Eq. (15). Eq. (17) is always valid for FT detection (since thermal diffusion can be neglected and the signal is given in general by $\alpha_a \int_0^\ell P(z)dz$). Eq. (17) formally proves the intuitive result that S is proportional to the absorptance of the sample. The expression $S \propto [1-(R+T)]$ is also valid for pulsed FT detection[15] of optically thin liquids in which the first peak of the transient PZT response yields the photoacoustic signal.

From Eq. (17) one can see by the following simple example that S is quite <u>insensitive</u> to scattering for optically thin media. For an isotropically scattering, optically thin medium ($\alpha\ell \ll 1$) (Fig. 5), $R \simeq \alpha_s \ell (1-r_o)/2$ and $T \simeq 1 - \alpha\ell + \alpha_s\ell(1+r_o)/2$ (See Eqs. (22a,b)). Hence, $S \propto [1-(R+T)] \simeq \alpha_a\ell$, whereas R and T measured alone are dominated by scattering.

On the other hand, for an optically thick medium for which T=0, $S \propto (1-R)$, and hence, the photothermal signal is, in principle, equivalent to a reflectance measurement in this limit. This result is in good agreement with the experimental findings of Ref. 16. These conclusions will be further elucidated by the results of Section III.

2. $\ell_{th} << \ell_{op}, \ell$

From Eq. (15), it follows in this limit of very short thermal length that

$$S \longrightarrow T_e(\omega)P_0\left\{\frac{\alpha_a}{kk_f(\kappa k+\kappa_f k_f)}\left[1+\frac{2(1+r_0)}{(1-r_0)}R\right]+\frac{\beta_s\chi}{\beta_f\kappa k^2}\left[1-(R+T)\right]\right\} \tag{18}$$

The first term is the signal contribution from the heat diffused into the fluid (within a thermal length) at the sample-fluid boundary. The heat is proportional to α_a times the total power in that region which has increased by the factor $[1+2R(1+r_o)/(1-r_o)]$ due to scattering. This factor can be derived from a simple argument. The total power at the boundary is given by $\hat{P}^-(0) + \hat{P}^+(0) + P_o$ where $\hat{P}^-(0)$ and $\hat{P}^+(0)$ are the backward and forward propagating diffuse photons/sec, respectively. But $\hat{P}^+(0) = r_0\hat{P}^-(0)$, and $\hat{P}^-(0) = 2RP_o/(1-r_o)$. Hence, $\hat{P}^+(0) + \hat{P}^-(0) + P_o = [1+2(1+r_o)/(1-r_o)R]P_o$. The second term in Eq. (18) (thermal expansion of the sample) can be significant at this high frequency limit[8] or for porous media.

3. Semi-infinite sample ($\ell \to \infty$)

In this limit, it is observed from Eqs. (5) and (6) that $\bar{\tau}(0) \underset{\ell\to\infty}{\longrightarrow} \frac{\alpha_a}{\kappa k(1+g)} \int_0^\infty P(z)\exp(-kz)dz$ and $\bar{\tau}(\ell) \underset{\ell\to\infty}{\longrightarrow} 0$. Using the above and Eq. (16) in Eqs. (1) and (4), we derive

$$S(\omega) = T_e(\omega)P_0\left\{\frac{\alpha_a[2R(2(\alpha_a+\alpha_s\Lambda)+k(\frac{1+r_0}{1-r_0}))(\alpha+k)+k^2-4\alpha(\alpha_a+\alpha_s\Lambda)+2n\alpha_s k]}{k_f(\kappa k+\kappa_f k_f)\,[k^2-4\alpha_a(\alpha_a+\alpha_s\Lambda](\alpha+k)} + \frac{\beta_s\chi}{\beta_f\kappa k^2}(1-R)\right\} \tag{19}$$

Note that setting $k>>2\alpha$ in Eq. (19) leads to the limit in Sec. II(C)2 (Eq. (18) with T=0), and $k<<\alpha$ yields the limit in Sec. II(C)1 (Eq. (17) with T=0).

D. Reflectance and Transmittance

The solution for the photothermal signal in terms of the measurable optical properties of the sample (R and T) can be employed in either of two ways: (1) photoacoustic measurements can be combined with optical measurements to provide information on sample properties, such the internal reflectance (r_o), which is otherwise experimentally inaccessible; or (2) the radiative transfer equation (Eq. (8)) can be solved for R and T in terms of the intrinsic optical properties of the sample (α_a , α_s , scattering indicatrix and boundary reflectances). Substituting these expressions for R and T into the general solution for the photothermal signal, one obtains the dependence of the PTS on the scattering and absorption of the sample.

The well-developed numerical techniques of radiative transfer theory[2,11,13] can be utilized for an accurate determination of R and T to be employed in Eqs. (15) and (17-19). However, the widely used three-flux (four-flux if the specular reflection at the $z=\ell$ boundary is non-negligible) calculations based on Eq. (11) have been observed and accepted to be sufficiently accurate.[17] Using this approach, we determine

$$R = \frac{(1-r_0)}{2D(\Gamma^2-\alpha^2)} \left\{ e^{-\Gamma\ell}\alpha_s(R_\infty-r_\ell)\ [-R_\infty((\alpha_a-\alpha_s)(1-\eta)+2\alpha_s\Lambda)+(3\alpha_a+\alpha_s)(1+\eta)+2\alpha_s\Lambda] \right.$$

$$+ e^{\Gamma\ell}\alpha_s(1-r_\ell R_\infty)\ [(\alpha_a-\alpha_s)(1-\eta)+2\alpha_s\Lambda-R_\infty((3\alpha_a+\alpha_s)(1+\eta)+2\alpha_s\Lambda)]$$

$$\left. + e^{-\alpha\ell}(1-R_\infty^2)\ [2r_{c\ell}(\Gamma^2-\alpha^2)-\alpha_s((\alpha_a-\alpha_s)(1-\eta)+2\alpha_s\Lambda \right.$$

$$\left. -r_\ell((3\alpha_a+\alpha_s)(1+\eta)+2\alpha_s\Lambda))] \right\} \qquad (20)$$

$$T = \frac{1}{2D(\Gamma^2-\alpha^2)} \left\{ (1-r_\ell)(1-R_\infty^2)\alpha_s\ [r_0(\alpha_a-\alpha_s)(1-\eta)-2\alpha_s\Lambda(1-r_0)-(3\alpha_a+\alpha_s)(1+\eta)] \right.$$

$$+ e^{-(\alpha+\Gamma)\ell}(r_0-R_\infty)\ [\alpha_s(1-r_\ell)(R_\infty(1+\eta)(3\alpha_a+\alpha_s)-2\alpha_s\Lambda(1-R_\infty)$$

$$- (\alpha_a-\alpha_s)(1-\eta))+2P_0(\Gamma^2-\alpha^2)(r_{c\ell}-r_\ell+R_\infty(1-r_{c\ell}))]$$

$$+ e^{-(\alpha-\Gamma)\ell}(1-r_0R_\infty)\ [\alpha_s(1-r_\ell)((3\alpha_a+\alpha_s)(1+\eta)+2\alpha_s\Lambda(1-R_\infty)$$

$$\left. - R_\infty(\alpha_a-\alpha_s)(1-\eta))+2P_0(\Gamma^2-\alpha^2)(1-r_{c\ell}+R_\infty(r_{c\ell}-r_\ell))] \right\} \qquad (21)$$

where

$$\Gamma = 2\sqrt{\alpha_a(\alpha_a+\alpha_s\Lambda)} \quad , \quad R_\infty = (2\alpha_a+\alpha_s\Lambda-\Gamma)/\alpha_s\Lambda$$

and

$$D = (1-r_\ell R_\infty)(1-r_0R_\infty)e^{\Gamma\ell} - (R_\infty-r_\ell)(R_\infty-r_0)e^{-\Gamma\ell}$$

III. Results and Discussion

In Eqs. (15), (20), and (21), which determine the photothermal signal, there are five optical constants, r_o, r_ℓ, $r_{c\ell}$, Λ, and η, in addition to the fundamental constants α_a and α_s. The values of these five constants can be judiciously chosen from theoretical considerations.[17] The boundary reflectances r_o and r_ℓ can be set equal to their theoretical values for perfectly diffuse light using the refractive index of the material.[17] In general, $r_{c\ell}=0$, but the diffuse reflectance characteristics of the backing medium must be taken into account. For example, if the backing medium is a highly diffuse reflector,[14] $r_\ell \simeq r_{c\ell} \simeq 1$ (also $T=0$). The parameters Λ and η take into account the anisotropy of scattering and can be deduced from the scattering indicatrix. For a given λ/d, one can determine $s(\psi) = s(\theta - \theta')$ from Mie formulae[18] (spherical particles) and evaluate its Legendre expansion coefficients $a_\ell = (2\ell+1)\int_{-1}^{1} s(\psi) P_\ell(\cos\psi) d(\cos\psi)$. Then from Eqs. (10) and (11), one can set $\eta \simeq (a_1 - a_3/4 + a_5/8)/2$ and $\Lambda \simeq 1 - a_1/4 - a_3/64$ with good accuracy. Thus, the only unknown parameters remaining are the important optical constants α_a and α_s.

In Fig. 6, the dependence of PTS on the optical thicknesses of the sample $\alpha_a \ell$ and $\alpha_s \ell$ is given for the low frequency and high frequency limits (Eq. (17) and (18)). Eqs. (20) and (21) are used with isotropic scattering ($\Lambda=1$, $\eta=0$). It is seen that the photothermal signal is not significantly affected for $\alpha_s \ell \ll 1$. In fact, it can be shown from Eqs. (20) and (21) that for $\alpha\ell \ll 1$

$$S \underset{\omega\to 0}{\longrightarrow} 1 - (R+T) \simeq \alpha_a \ell \tag{22a}$$

$$S \underset{\omega\to\infty}{\longrightarrow} \alpha_a\left[1 + \frac{2(1+r_0)}{(1-r_0)} R\right] \simeq \alpha_a[1+(1+r_0)\Lambda\alpha_s\ell] \tag{22b}$$

Therefore, Fig. 6 and Eqs. (22a,b) demonstrate that, for the wide range of techniques considered, PTS is independent of scattering for $\alpha_s \ell \lesssim 0.1$. This result is not evident from the analysis of Helander et al.[4] who only considered semi-infinite, and therefore optically thick, samples. They found that PTS was very sensitive to scattering when $\alpha_s \geq \alpha_a$. For larger $\alpha_s \ell$, it is seen from Fig. 6 that S is significantly affected, initially increasing with $\alpha_s \ell$, and eventually decreasing for very large $\alpha_s \ell$.

Physically, for $\alpha_s \ell << 1$, the effective light path length within the sample is equal to its thickness, and the PTS is not affected. When $\alpha_s \ell \sim 1$ the mean path length of light increases and so does the absorption. At still higher scattering, the signal saturates as a function of $\alpha_s \ell$ since all the light is scattered without further increase in the effective path lengths. For very high scattering samples ($T \simeq 0$), the reflectance becomes larger as $\alpha_s \ell$ is increased leading to a decrease in the light intensity within the sample. Hence, the signal decreases.

For the thermally thick case, the signal rises as $\alpha_s \ell$ increases above 0.1 since scattering increases the flux at the surfaces (increases R). For $\alpha_s \ell >> 1$, $R \simeq 1$ (the surface flux can no longer increase), and the signal saturates at the level $\alpha_a \ell (1+2(1+r_o)/(1-r_o))$.

Note that, in the region $\alpha_s \ell \sim 1$, S monotonically increases as a function of $\alpha_s \ell$ for a fixed $\alpha_a \ell$ (up to a factor of ~ 5 for $\alpha_a \ell < 0.1$). The scattering coefficient α_s is a decreasing function of λ/d for $\lambda/d \gtrsim 1$. (The dependance of α_s on λ/d is given by the Rayleigh and Mie scattering formulae.[18]) Hence, for a fixed mean particle diameter and absorption coefficient, S may increase significantly as λ is decreased to approach

$\lambda = d$, if $0.1 \leq \alpha_s \ell \leq 10$. For submicron particle sizes, this implies that there may be a monotonic increase in S as λ is decreased towards the UV if $\alpha_s \ell \sim 1$.

In Figs. (7) and (8), the ratio $R_0 = S(\alpha_s \neq 0)/S(\alpha_s = 0)$ is plotted as a function of $\alpha_a \ell$ for varying $\alpha_s \ell$, assuming isotropic scattering and neglecting the mechanical expansion, in the low and high frequency limits. The results of Fig. 7 can be explained as follows: (1) for low scattering ($\alpha_s \ell > 0.1$) and low absorption, the mean path through the sample is slightly increased, giving light a greater chance of being absorbed and resulting in $R_0 > 1$; (2) when the absorption increases sufficiently, the light is absorbed regardless of whether it scatters, so $R_0 \rightarrow 1$; (3) for very high scattering and low absorption, the light is more likely to be scattered out of the sample than to be absorbed, giving, $R_0 < 1$; (4) as the absorption becomes larger than the scattering, the light absorption probability increases, giving $R_0 \rightarrow 1$. For Fig. 8, scattering increases the surface intensity up to a point, but for very high absorption the surface intensity decreases. Another important observation evident from Figs. 7 and 8 is that the general effect of scattering on a spectrum is to lower the peaks and raise the valleys.

In Fig. 9 and 10, curves of $\alpha_a \ell$ (measured) versus $\alpha_a \ell$ (actual) are given for the low frequency and high frequency limits (isotropic scattering). The physical interpretation is the same as in Figs. 7 and 8. These curves are useful for correcting spectra for the effects of scattering.

In Figs. (11-13), we compare our results with the experimental and theoretical results of Helander *et al.* [4] R_0 is computed using the

thermal properties of water and air from Eq. (19) and Eq. (20) ($\ell \to \infty$, T=0). We use the theoretical value of $r_o = 0.4$ (valid for uniformly diffused light incident on an interface with index ratio of n=1.33) which is more realistic[17] than the smaller value (r_o=0) used in Ref.4. Our curves for r_o=0 and isotropic scattering are very similar to those in Ref. 4 but are in better agreement with their data. Since the mean particle diameters used in Ref. 4 are comparable to the wavelength, the scattering indicatrix is likely to be peaked in the forward direction. Since we do not know the exact value of λ/d, we estimate $\Lambda = 0.5$, $\eta = 0.5$. Our results are in reasonably good agreement with their experimental measurements. In Fig. 11, the data

may involve the changing of Λ and η as α_s is varied. This may explain the small discrepancy. A curve with $\Lambda = 0.2$, $\eta = 0.5$ agrees well with the data. In Figs. 12 and 13, the scattering properties are not being changed, and we obtain better agreement. Noting that the realistic value of r_o=0.4 is used, the agreement is remarkably good. One reason is that the mechanical expansion term is also included in our analysis and is not entirely negligible in their experiment.

In these computed curves, we made no attempt for a numerical fitting of parameters. Following the discussion at the beginning of this section, we chose reasonable values based on theoretical considerations. If more accurate values of the parameters were available, better agreement could be obtained.

The above theoretical results suggest the following ways to optimize PTS of scattering media. First, the scattering properties of the solid should be kept constant, and hence, the particle size must not

change drastically from sample to sample. Second, because scattering flattens out spectral features, it should be minimized by keeping the particle size small or by immersion in a liquid. Third, one can attempt to estimate the scattering length and use Figs. 9 and 10 to correct the signal. The curves may not be appropriate for every experimental configuration since the curves were generater neglecting the mechanical term and assume isotropic scattering. Forth, if $\alpha_a \ell > .01$ and the sample is optically thick, diffuse reflectance measurements give equivalent results and may be more convenient than PTS; for weakly absorbing samples, PTS gives better results.

In conclusion, we have shown that while photothermal spectroscopy is independent of scattering for optically thin media, it is significantly affected by scattering in general and is equivalent to diffuse reflectance spectroscopy in some limits. However, the general photothermal signal contains information which is not available by optical means and which can be measured by variation of the chopping frequency. By parameter fitting our theoretical curves to the frequency dependent photothermal data, α_a and α_s can be numerically estimated. Optical measurements of R and T can be used to supplement this procedure. Utilized in this manner, photothermal spectroscopy can be an important tool for the determination of optical constants for highly scattering media.

Acknowledgements

We thank R. Gerlach for helpful discussions. This work was supported by the Office of Energy Research, Pollution Characterization and Measurement Division of the U.S. Department of Energy under Contract W-7405-ENG-48.

Appendix: Solid-Transducer (ST) Detection

From the expression $G(\vec{r}) = 1 \pm 3\,(1 - 2z/\ell)$ for the ST (PZT)[10] scheme, it follows that

$$S_{PZT}(\omega) = T_e(\omega)\left[\int_0^\ell \bar{\tau}(z)dz \pm 3\int_0^\ell (1 - \frac{2z}{\ell})\bar{\tau}(z)dz\right] \tag{A1}$$

The first term in brackets represents the thermal expansion of the sample and is given by Eq. (4) in the main text. To evaluate the second term, which represents the sample buckling due to the average temperature gradient along z, we multiply Eq. (2) by z and integrate, obtaining

$$k^2\int_0^\ell z\bar{\tau}(z)dz = \frac{\alpha_a}{\kappa}\int_0^\ell zP(z)dz - (1+\ell\,\frac{\kappa_b k_b}{\kappa})\bar{\tau}(\ell) + \bar{\tau}(0)$$

Using the above and Eq. (4) in (A1), we obtain

$$S_{PZT}(\omega) = \frac{T_e(\omega)}{\kappa k^2}\left\{(1\pm3)\alpha_a\int_0^\ell P(z)dz \mp \frac{6}{\ell}\,\alpha_a\int_0^\ell zP(z)dz\right. \tag{A2}$$

$$\left.(-1\pm3)\kappa_b k_b\bar{\tau}(\ell) - (1\pm3)\kappa_f k_f\bar{\tau}(0) \pm \frac{6}{\ell}\,\kappa(\bar{\tau}(0) - \bar{\tau}(\ell))\right\}$$

where,

$$\int_0^\ell zP(z)dz = \int_{-1}^{1} d\mu\int_0^\ell zP_d(z,\mu)dz + \frac{1}{\alpha^2}\,P_0[1-(1+\alpha\ell)\exp(-\alpha\ell)]$$

Multiplying Eq. (8) by z and integrating over $-1 \le \mu \le 1$ and $0 \le z \le \ell$ gives

$$\ell[\Phi^+(\ell)-\Phi^-(\ell)] - \int_{-1}^{1}\mu d\mu\int_0^\ell P_d(z,\mu)dz = -\alpha_a\int_0^\ell zP(z)dz + \frac{1}{\alpha}\,P_0[1-(1+\alpha\ell)\exp(-\alpha\ell)]$$

Applying the Schuster-Schwarzchild approximation (Eq.(11)) and using Eq. (14), the above equation can be written as

$$\alpha_a \int_0^{\ell} zP(z)dz = \frac{1}{2}\,(P_d^+ - P_d^-) + \frac{P_0}{\alpha}\,[(1-\exp(-\alpha\ell))-\alpha\ell T] \qquad \text{(A3)}$$

where

$$P_d^+ \equiv \int_0^1 d\mu \int_0^{\ell} dz P_d(z,\mu) \qquad \text{and} \qquad P_d^- \equiv \int_{-1}^0 d\mu \int_0^{\ell} dz P_d(z,\mu) \quad .$$

From the equations following Eq. (11), we obtain

$$(\alpha_a+\alpha_s\Lambda)(P_d^+-P_d^-) = \Phi^+(0)+\Phi^-(0) - (\Phi^+(\ell)+\Phi^-(\ell))+ n\,\frac{\alpha_s}{\alpha}\,P_0(1-\exp(-\alpha\ell))$$

which, using Eq. (13) and Eq. (14), can be rewritten as ($r_{c\ell} = 0$)

$$(\alpha_a+\alpha_s\beta)(P_d^+-P_d^-) = P_0\left[n\,\frac{\alpha_s}{\alpha}\,(1-\exp(-\alpha\ell)) + \left(\frac{1+r_0}{1-r_0}\right)R - \left(\frac{1+r_\ell}{1-r_\ell}\right)\,(T-\exp(-\alpha\ell))\right]$$

Substituting into Eq. (A3) gives

$$\alpha_a \int_0^{\ell} zP(z)dz = \frac{P_0}{\alpha}\,[(1-\exp(-\alpha\ell))-\alpha\ell T] \qquad \text{(A4)}$$

$$+ \frac{P_0}{2(\alpha_a+\alpha_s\Lambda)}\left[n\,\frac{\alpha_s}{\alpha}\,(1-\exp(-\alpha\ell) + \left(\frac{1+r_0}{1-r_0}\right)R - \left(\frac{1+r_\ell}{1-r_\ell}\right)\,(T-\exp(-\alpha\ell))\right]$$

Using Eqs. (A4), (5), (6), (15) and (16), Eq. (A2) yields the PZT signal in terms of the chopping frequency and the thermal and optical properties of the sample.

References

(a) Present address: Xerox Palo Alto Research Center, Palo Alto

(1) A. Rosencwaig, Analytical Chem., 47, 592A (1975).

(2) H. C. Van de Hulst, Multiple Light Scattering I (Academic Press, New York, 1980).

(3) G. Kortum, Reflectance Spectroscopy (Springer-Verlag, Berlin, 1969).

(4) P. Helander and I. Lundstrom, J. Appl. Phys. 51 3841 (1980).

(5) W. B. Jackson, N. M. Amer, A. C. Boccara, and D. Fournier, Appl. Opt. 20, 1333, (1981).

(6) J. P. Monchalin, L. Bertrand, J. L. Parpal and J. M. Gagne, Topical Meeting on Photoacoustic Spectroscopy, Berkeley, California (1981).

(7) P. Morse and K. Ingard, Theoretical Acoustics (McGraw-Hill, New York, 1968).

(8) F. A. Mcdonald, J. Opt. Soc. Am., 70 555 (1980).

(9) L. B. Kreuzer, Photoacoustic Spectroscopy and Detection, edited by Y.-H. Pao (Academic, New York, 1977).

(10) W. B. Jackson, and N. M. Amer, J. Appl. Phys. 51, 3343 (1980).

(11) S. Chandrasekhar, Radiative Transfer (Dover, New York, 1960).

(12) F. Kottler, Progress in Optics III, edited by E. Wolf (Wiley, New York, 1964).

(13) V. V. Sobolev, Light Scattering In Planetary Atmospheres (Pergamon, Oxford, 1975).

(14) Z. A. Yasa, N. M. Amer, H. Rosen, A. D. Hansen, and T. Novakov, Appl. Opt. 18, 2528 (1979).

(15) A. C. Tam, C.K. N. Patel, and R. J. Kerl, Opt. Lett. 4, 81 (1979).

(15) V. V. Sobolev, Light Scattering In Planetary Atmospheres (Pergamon, Oxford, 1975).

(16) J. J. Freeman, R. M. Friedman and H. S. Reichard, J. Phys. Chem. 84, 315 (1980).

(17) P. S. Mudgett and L. W. Richards, Appl. Opt. 10, 1485 (1971).

(18) H. C. Van de Hulst, Light Scattering by Small Particles (Wiley, New York, 1957).

Figure Captions

Fig.1 The cw photothermal techniques considered in this paper: (a) Sample-Fluid-Transducer (SFT) Technique (non-resonant). If the fluid is a gas, this describes the Sample-Gas-Microphone (SGM) technique. If the fluid is a liquid, the transducer (hydrophone) is usually a PZT. (b) Fluid-Transducer (FT) technique (resonant or non-resonant). For a gas, it describes the Gas-Microphone spectrophone. For a liquid, the transducer is generally a PZT. (c) Solid-Transducer (ST) Technique (non-resonant). The sample is epoxied to a flat PZT transducer which has a hole at the center to minimize the scattered light directly hitting the transducer. The beam can be incident from either side.[10] (d) Transverse-Photothermal Deflection (PDS) technique. The pump beam of radius, w_o, is normally incident on the sample. A probe beam of much smaller radius propagates parallel to the sample a distance z_o away from the surface and through the center of the pump beam. The deflection of the probe beam is given by the average temperature gradient along its propagation path.[5]

Fig.2 The typical sample geometry. ℓ is the length of the sample. The fluid and backing regions are assumed to be thermally thick.

Fig.3 Diffuse photons/sec at position z, propagating in directions θ ($\cos\theta = \mu$) and θ' ($\cos\theta' = \mu'$) relative to the z-axis.

Fig.4 Description of the special cases (1) and (2). (a) and (b) describe the case in Sec. II(C)1 (c) is the case in Sec. II(C)2.

Fig.5 An optically and thermally thin ($\alpha\ell << 1$) medium with the internal reflectances $r_o \neq 0$, $r_\ell = 0$ and isotropic scattering. The photothermal signal is given by $S \propto [\, 1-(R+T)\,] \simeq \alpha_a \ell$.

Fig.6 Relative photothermal signal versus scattering, $\alpha_s \ell$, for various absorptions, $\alpha_a \ell$. $r_o = 0.6$, $r_\ell = r_{c\ell} = 0$ and $\Lambda = 1$, $\eta = 0$ (isotropic scattering). —— Theory (thermally thin), — — Theory (thermally thick). Note the independence of scattering for $\alpha_s \ell \leq .2$

Fig.7 R_o (ratio of signal with scattering to signal without) vs. absorption ($\alpha_a \ell$) for various values of $\alpha_s \ell$. The curves apply for the thermally thin limit (Eq. 17), isotropic scattering ($\Lambda = 1$, $\eta = 0$) and $r_o = 0.6$, $r_\ell = r_{c\ell} = 0$.

Fig.8 R_o versus absorption, $\alpha_a \ell$, for various values of $\alpha_s \ell$. The thermally thick limit (Eq. (18)) with the mechanical expansion term neglected. Isotropic scattering ($\Lambda = 1$, $\eta = 0$) and $r_o = 0.6$, $r_\ell = r_{c\ell} = 0$.

Fig.9 $\alpha_a \ell$ (measured) (neglecting scattering) versus $\alpha_a \ell$ (actual) for various values of $\alpha_s \ell$ for the thermally thin limit (Eq. 17). Isotropic scattering ($\Lambda = 1$, $\eta = 0$) and $r_o = 0.6$, $r_\ell = r_{c\ell} = 0$.

Fig.10 $\alpha_a \ell$ (measured) (neglecting scattering) versus $\alpha_a \ell$(actual) for various values of $\alpha_s \ell$ for the thermally thick limit (Eq. (18) with $\chi = 0$). Isotropic scattering ($\Lambda = 1$, $\eta = 0$) and $r_o = 0.6$, $r_\ell = r_{\ell'} = 0$.

Fig.11 R_0 versus chopping frequency for different absorption coefficients. —— present theory, - - - theory from Ref.4, Δ - $\alpha_a = 69$ cm^{-1} data, ¤ - $\alpha_a = 138$ cm^{-1} data, • - $\alpha_a = 276$ cm^{-1} data. Data is from Ref. 4. $\alpha_s = 1145$ cm^{-1}, $r_o = .4$, $\Lambda = \eta = 0.5$ and the thermal properties of water were used in the calculations.

Fig.12 R_0 versus absorption coefficient. — present theory, - - theory (Ref. 4). ⋄ - data (Ref.4) $\alpha_s = 500$ cm^{-1}, $r_o = .4$, f = 150 Hz, $\Lambda = \eta = .5$. Thermal properties of water were used in the calculations.

Fig.13 R_0 versus scattering coefficient. 1 - theory ($\alpha_a = 34.5$ cm^{-1}, $\Lambda = \eta = .5$), 2 - theory ($\alpha_a = 69$ cm^{-1}, $\Lambda = \eta = .5$), 3 - theory ($\alpha_a = 34.5$ cm^{-1}, $\Lambda = .2$, $\eta = .5$). 4 - data (Ref.4, $\alpha_a = 34.5$ cm^{-1}), 5 - data (Ref.4, $\alpha_a = 69$ cm^{-1}) 6 - theory (Ref.4) $\alpha_a = 34.5$ cm^{-1}, 7 - theory (Ref.4) $\alpha_a = 69$ cm^{-1}. The other parameters are f= 150 Hz, $r_o = 0.4$ and thermal properties of water and air.

TABLE I Definition of Parameters for Various PTS Methods

Method	$T_R(\omega)$ (Transducer sensitivity)	$T_t(\omega)$	$G(z,\rho,\phi)$	Description of parameters (f-fluid, s-sample)
Sample-Fluid -Transducer (SFT)	Volts/dyne/cm^2	$\dfrac{\beta_f}{VK_{Tf}}$	$\dfrac{\delta(z)}{k_f} + \dfrac{\beta_s}{\beta_f}\chi$	K_T - isothermal compressibility β - coefficient of thermal expansion k - $(1+i)(\omega\rho C_p/2\kappa)^{\frac{1}{2}}$, κ - thermal conductivity ω - modulation frequency ρC_p - heat capacity/unit volume at constant pressure V - cell volume ρ - density γ - ratio of specific heats
Fluid-Transducer (FT) (a) Non-resonant (b) Resonant	Volts/dyne/cm^2	$\dfrac{\beta}{K_T V}$ $\dfrac{i2\beta}{Q_j \pi V K_T J_o(\pi\alpha_j)}$	1 $J_o\left(\frac{\pi}{a}\alpha_j\rho\right) \to 1$	a - cell radius $\dfrac{d}{d_\alpha} J_o(\pi\alpha)\Big\|_{\alpha=\alpha_j} = 0$ Q_j = cavity Q(jth mode)
Solid-Transducer (ST)	Volts/ unit strain	$\beta(1+\nu)$	$1 \pm 3\left(1-\dfrac{2z}{\ell}\right)$	ℓ - sample length ν - poisson's ratio
Transverse Photothermal Deflection (PDS)	Volts/radian	$\dfrac{1}{n_o}\dfrac{dn}{dT}\sqrt{\dfrac{2}{\pi}}$ $\times k_f^2 \dfrac{e^{k_f z_o}}{w_o}$	$\dfrac{\delta(z)}{k_f}$	w_o - pump beam radius $\dfrac{1}{n_o}\dfrac{dn}{dT}$ - relative change of refractive index with temp.

TABLE II Effective Parameters for Porous Media[7]

Parameter	Effective Parameter	Remarks
K_T	$K_T\Omega$	Ω - Volume fraction of fluid (porosity)
β	β_e	Accounts for thermal and mechanical properties of the fluid sample system
κ	κ_e	
ρC_p	ρC_{pe}	
χ	$\Omega\left(\frac{1-i\phi}{\rho_p \omega}\right)$	ϕ - flow resistance (the ratio of the pressure drop across sample to velocity flow within sample)
V	$V\left[1+\frac{\gamma_f}{\gamma_s}\Omega\chi\right]$	Includes effects of fluid flow from sample
ρ	$\rho_p\left(1+\frac{i\phi}{\rho_p \omega}\right)$	Includes viscosity effects and particle motion within fluid

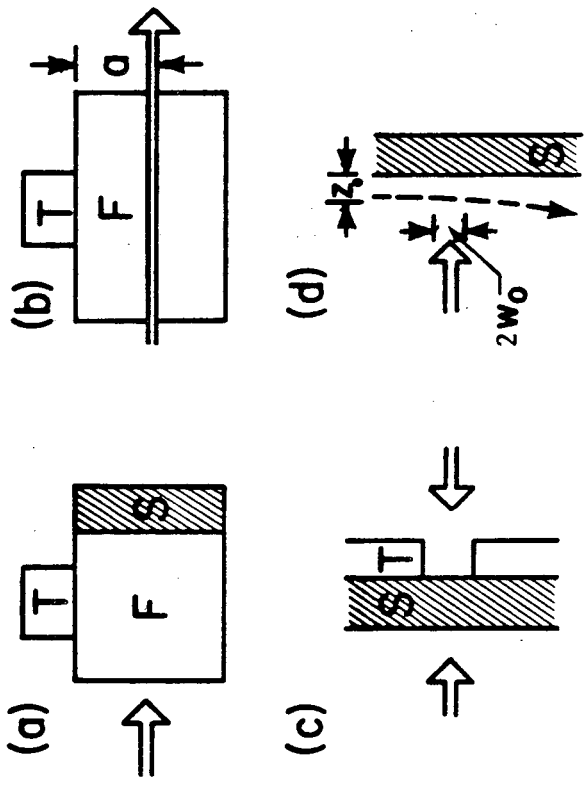

XBL 818-1274

Fig. (1)

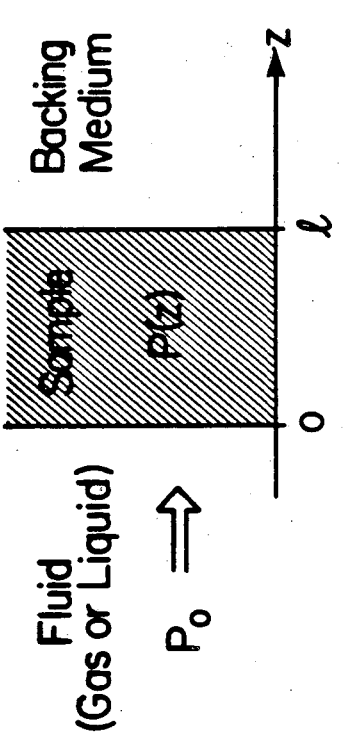

XBL 818-1273

Fig. (2)

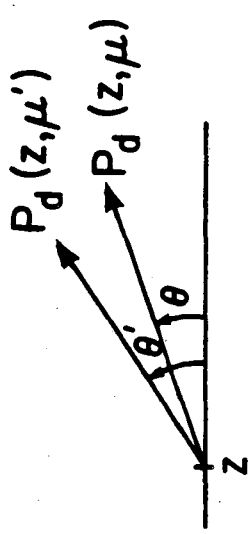

XBL 818-1272

Fig. (3)

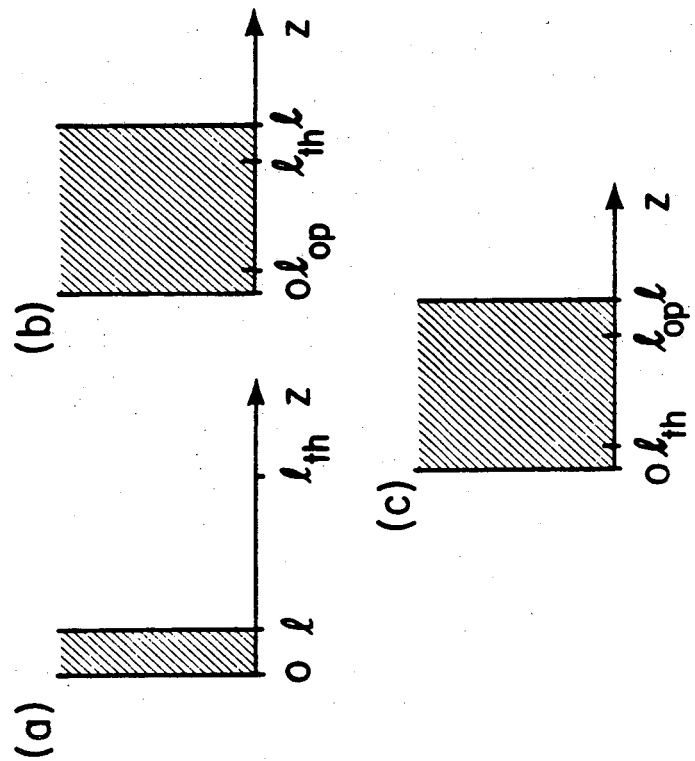

XBL 818-1275

Fig. (4)

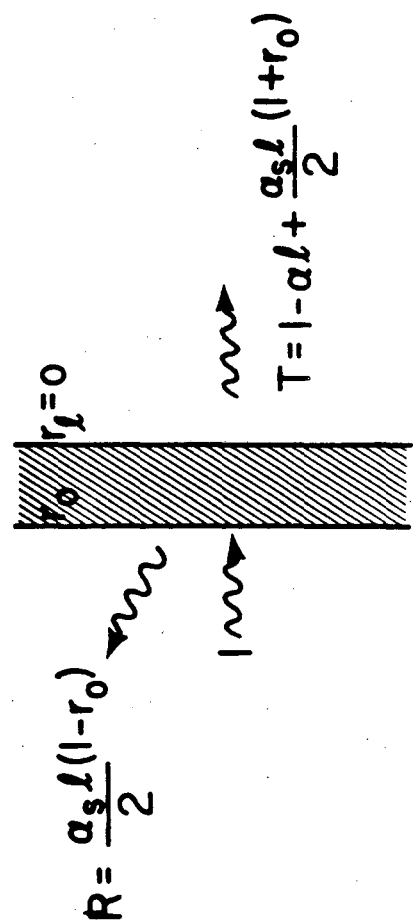

XBL 818-1271

Fig. (5)

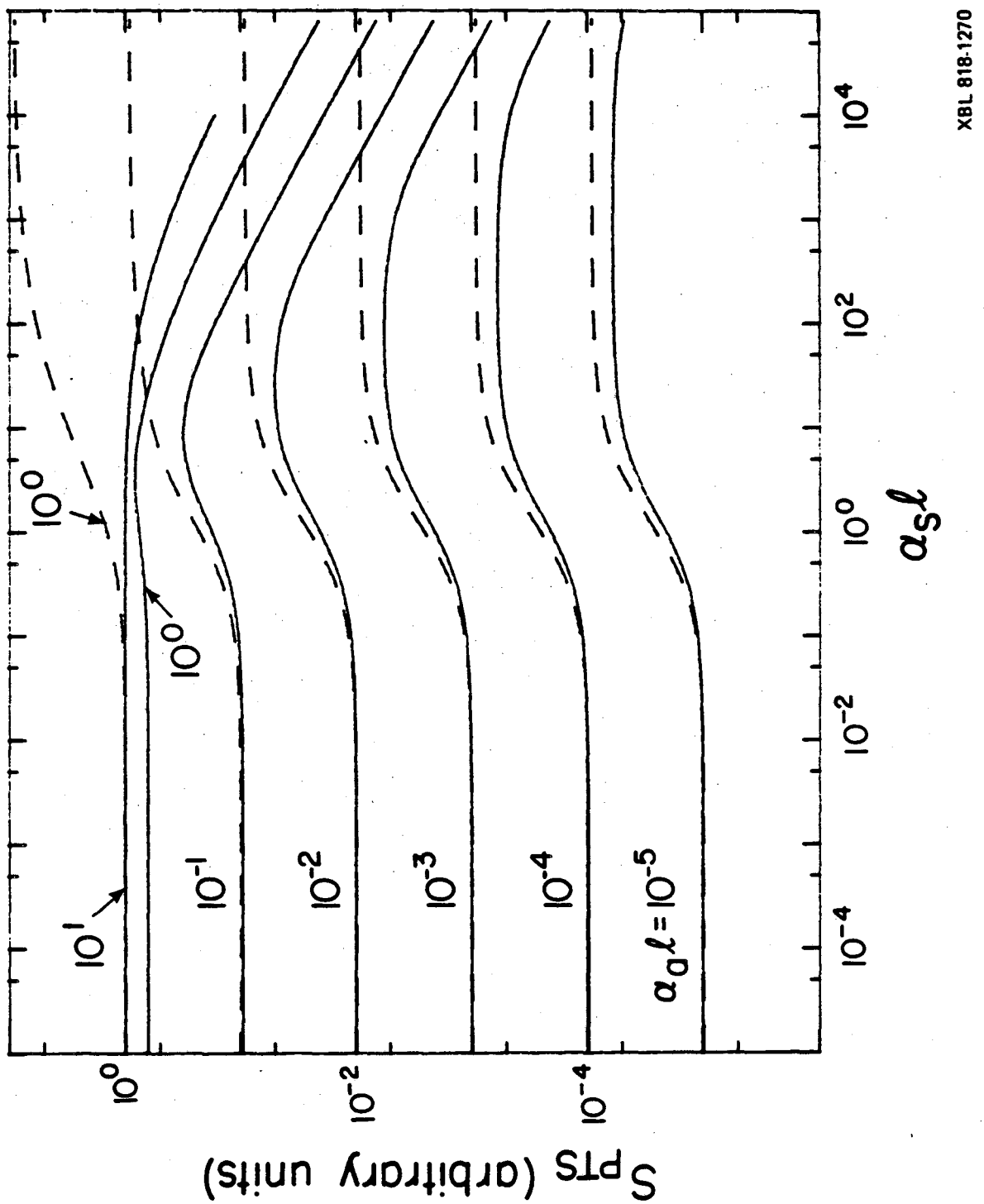
S_{PTS} (arbitrary units)
10^{0}
10^{-2}
10^{-4}
10^{1}
10^{0}
10^{-1}
10^{-2}
10^{-3}
10^{-4}
$\alpha_a \ell = 10^{-5}$
10^{-4}
10^{-2}
10^{0}
10^{2}
10^{4}
$\alpha_s \ell$
XBL 818-1270

Fig. (6)

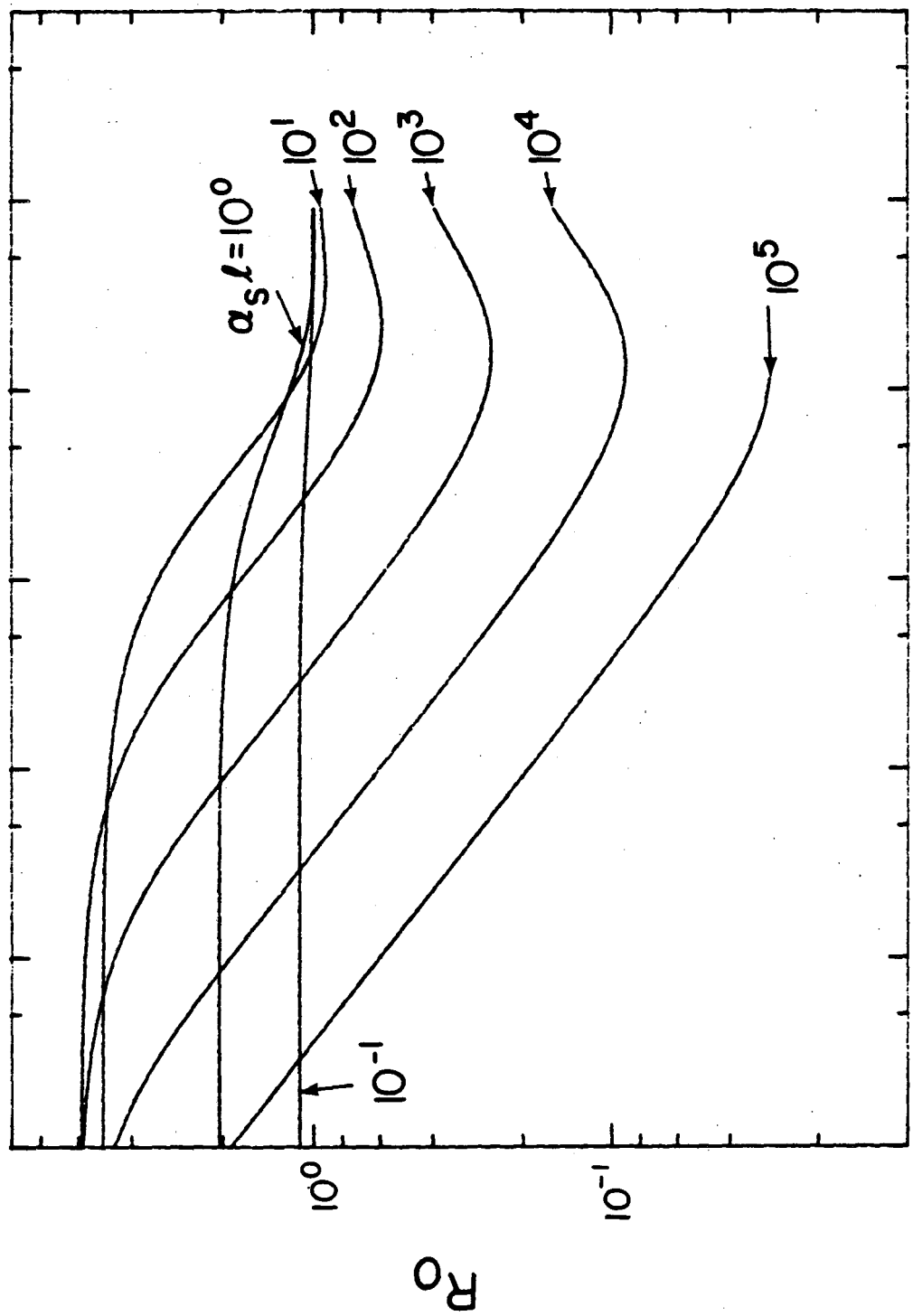
R_o
10^0
10^{-1}
10^{-1}
10^{-3}
10^1
$a_q \ell$
$a_s \ell = 10^0$
10^1
10^2
10^3
10^4
10^5
XBL 818-1269

Fig. (7)

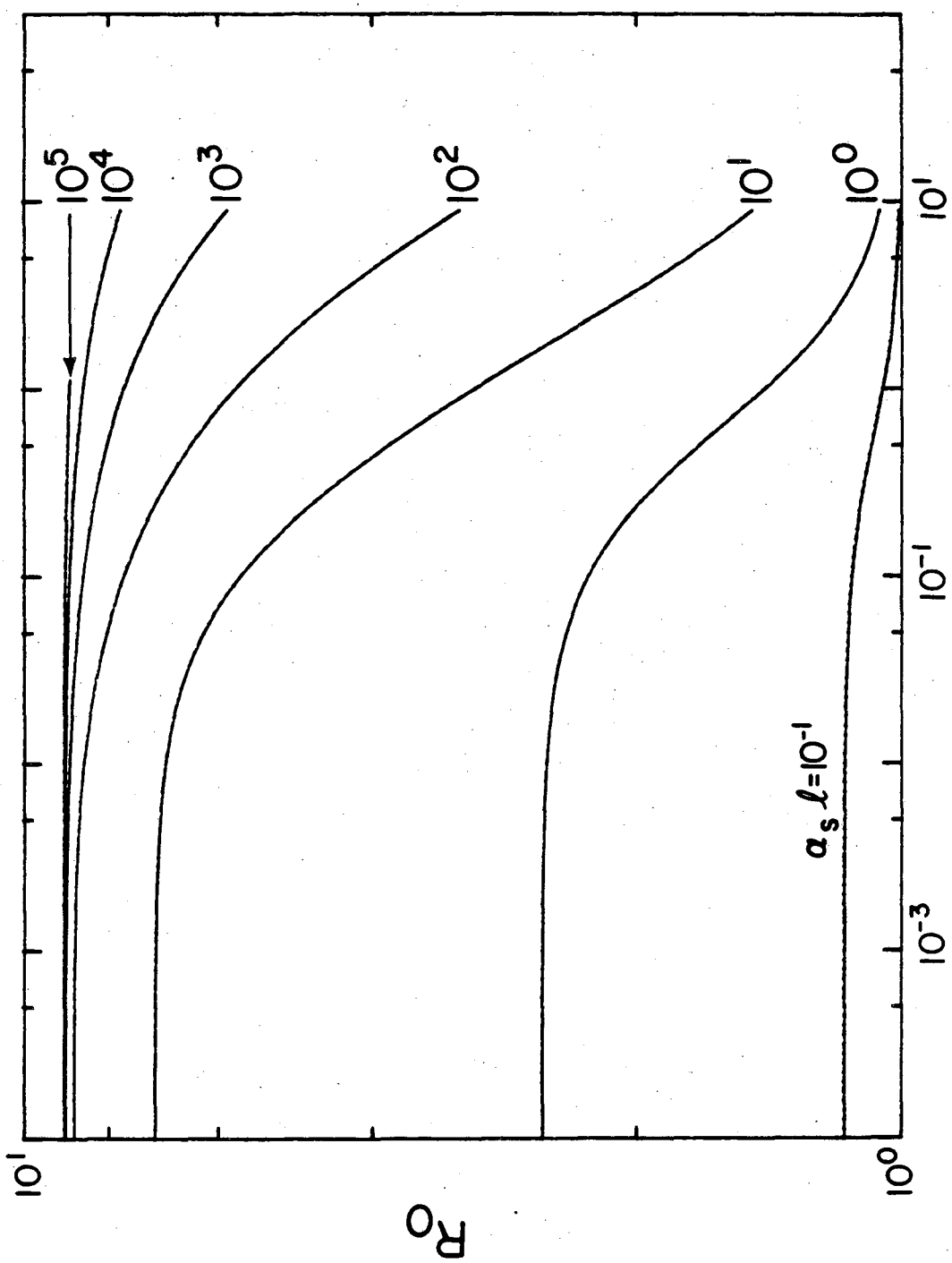
10^5
10^4
10^3
10^2
10^1
10^0
10^1
10^{-1}
10^{-3}
$a_s \ell = 10^{-1}$
R_0
10^1
10^0
$a_0 \ell$
XBL 818-1265

Fig. (8)

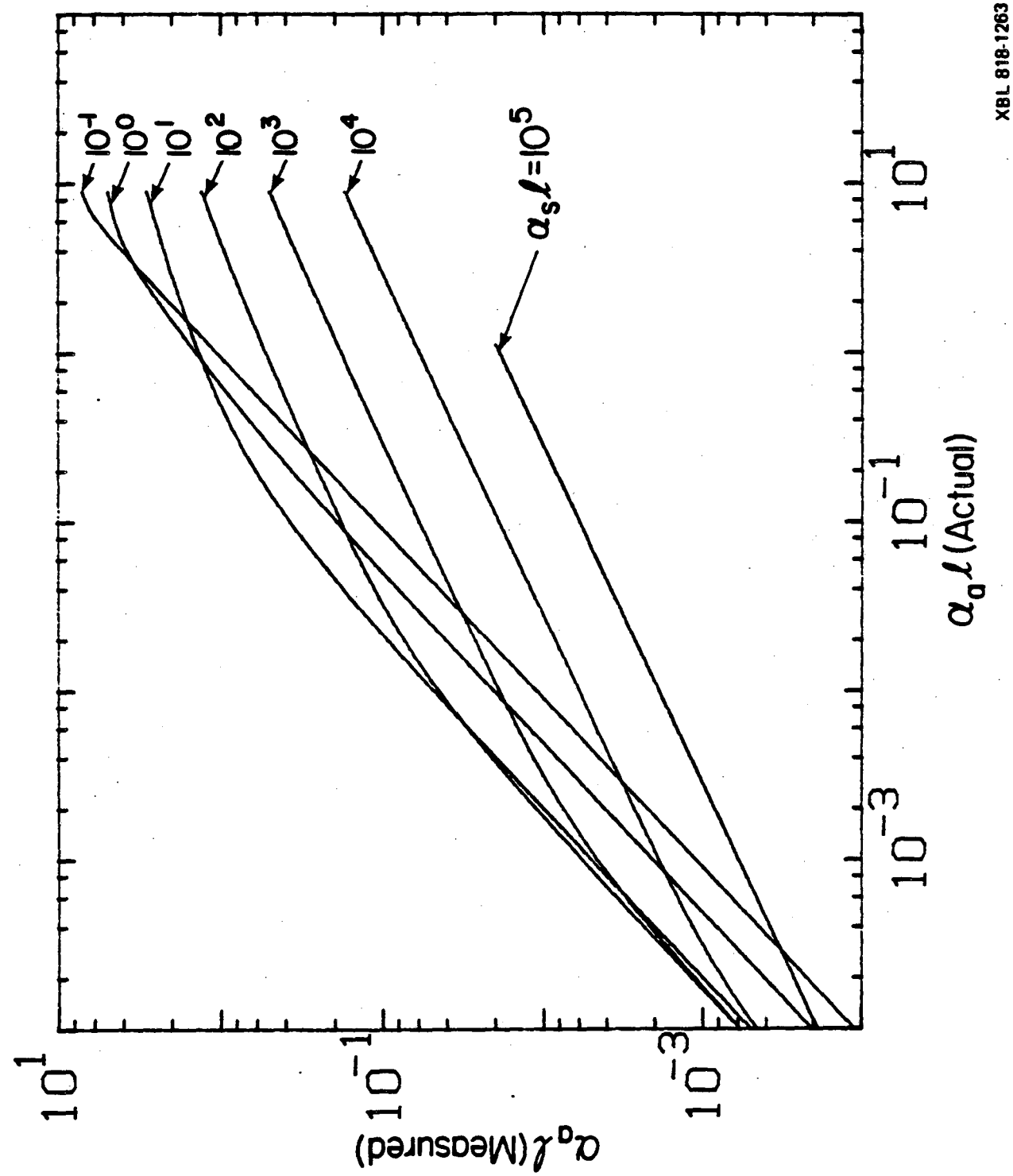
10^{-1}
10^{0}
10^{1}
10^{2}
10^{3}
10^{4}
$\alpha_s \ell = 10^{5}$
10^{1}
10^{-1}
10^{-3}
$\alpha_q \ell$ (Measured)
10^{-3}
10^{-1}
10^{1}
$\alpha_q \ell$ (Actual)
XBL 818-1263

Fig. (9)

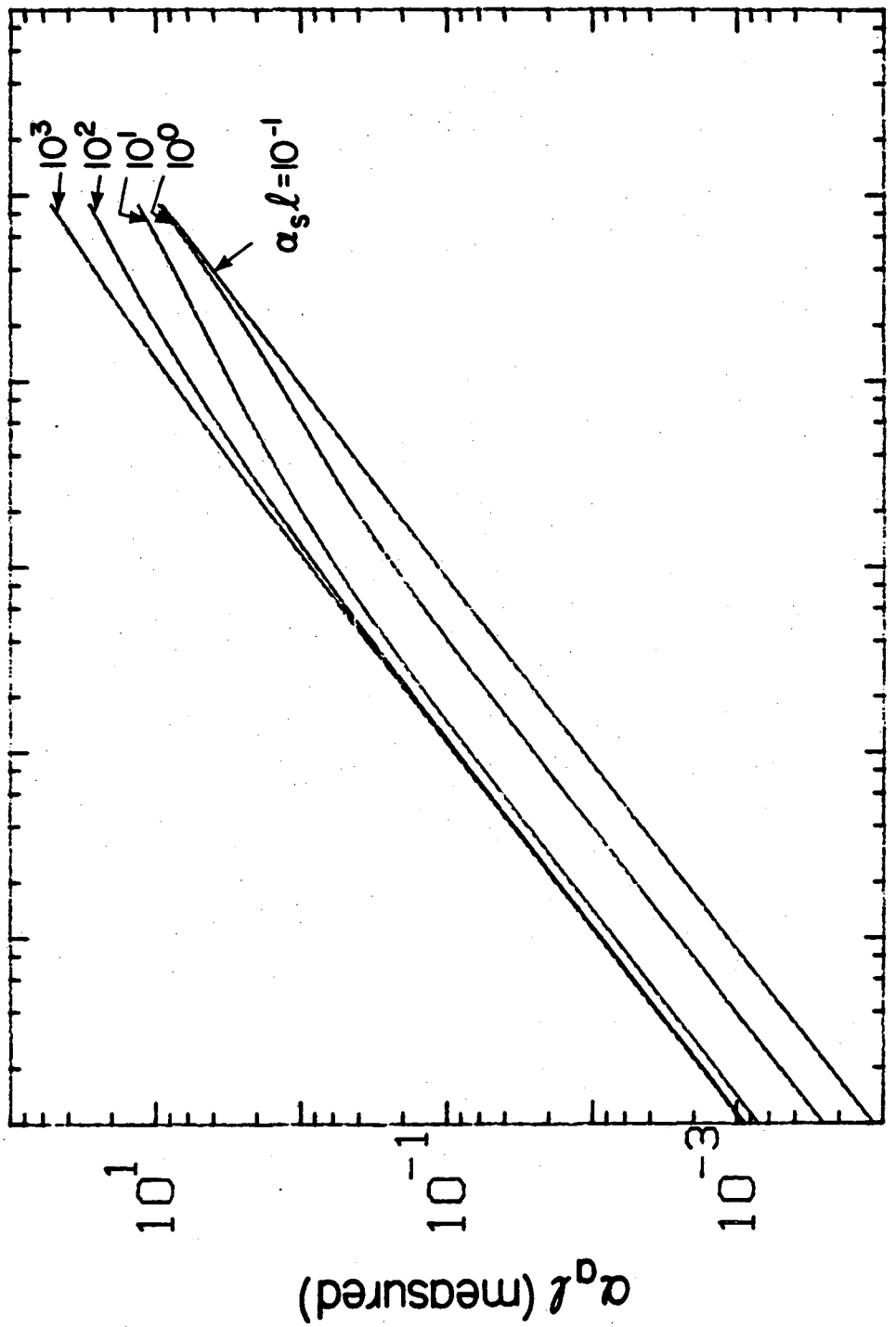
$\alpha_s \ell = 10^{-1}$
10^0
10^1
10^2
10^3
10^{-3}
10^{-1}
10^1
$\alpha_q \ell$ (Actual)
10^{-3}
10^{-1}
10^{-1}
$\alpha_q \ell$ (measured)
XBL 818-1266

Fig. 10

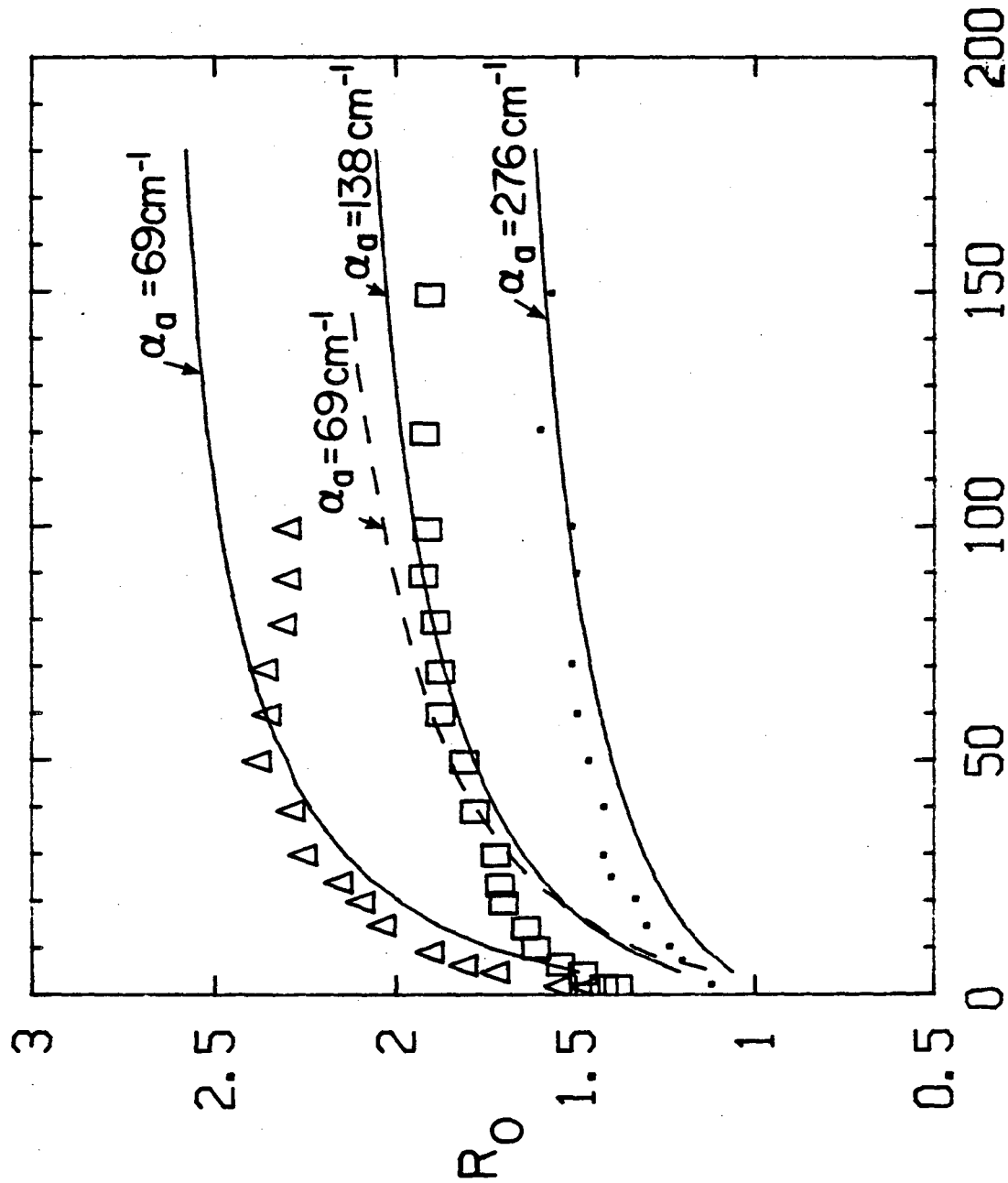

XBL 818-1264

Fig. (11)

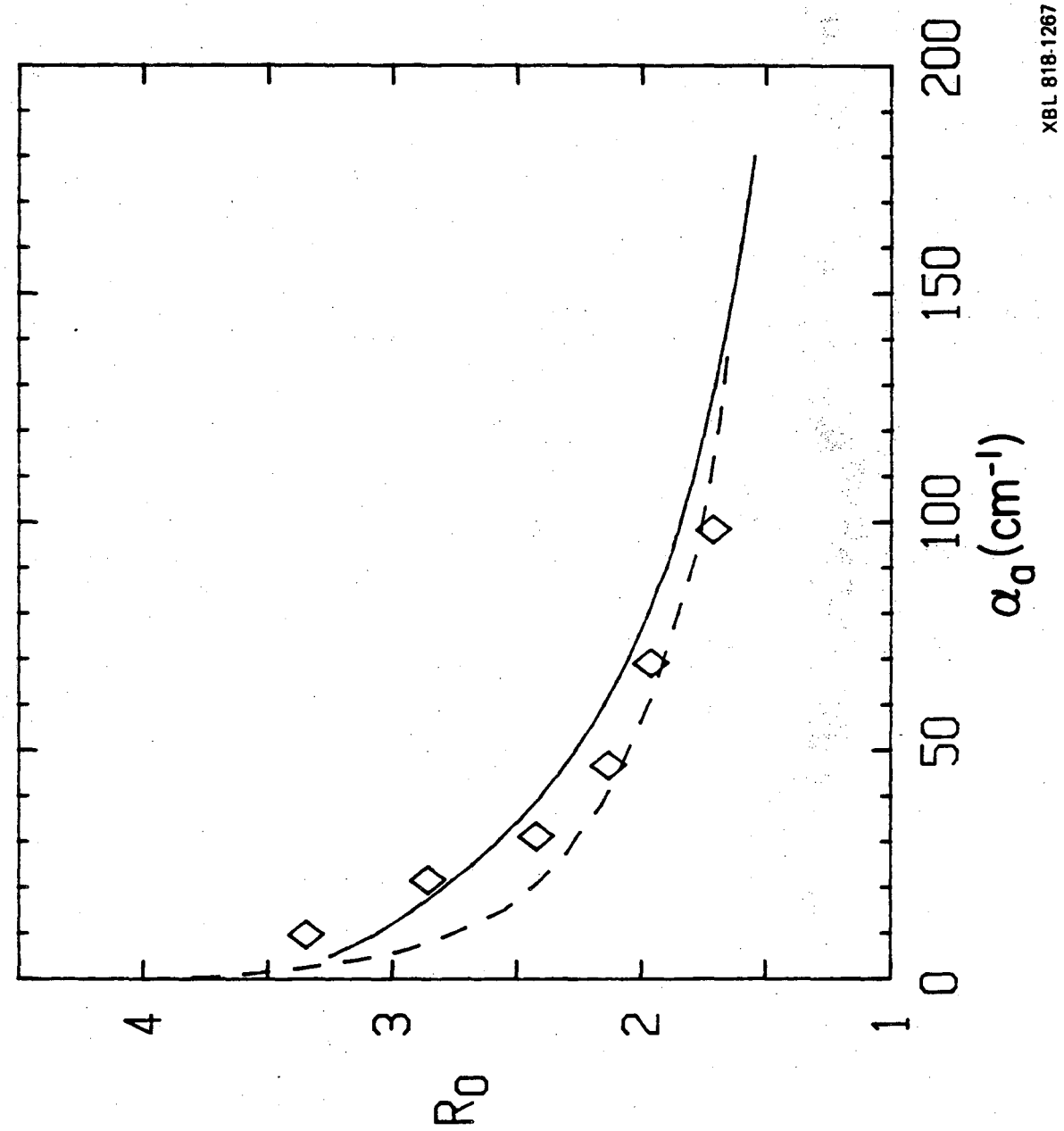

Fig. (12)

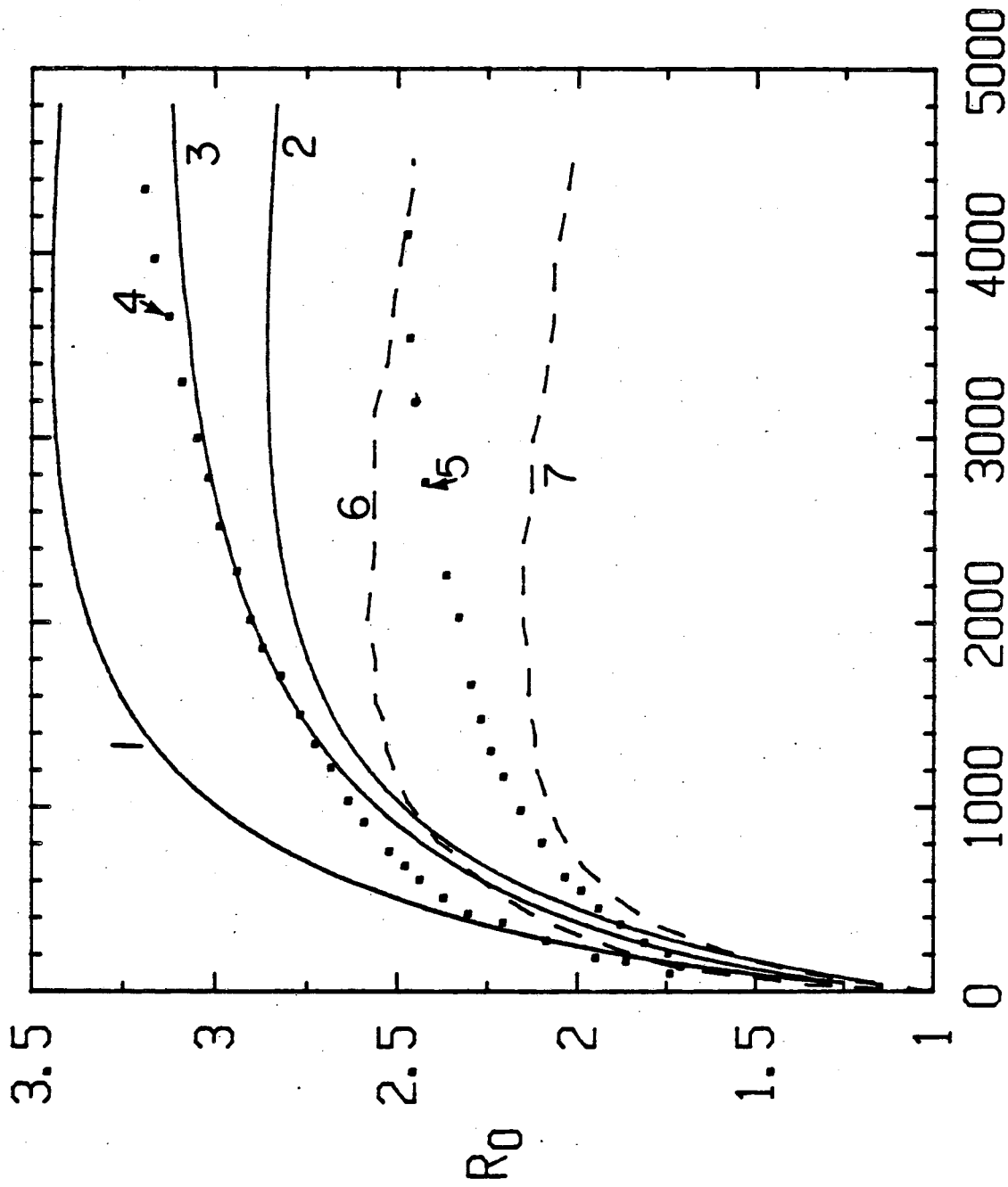
3.5
3
2.5
2
1.5
1
R_0
0
1000
2000
3000
4000
5000
$\alpha_s(cm^{-1})$
1
2
3
4
5
6
7
XBL 818-1268

Fig. (13)

TECHNICAL INFORMATION DEPARTMENT
LAWRENCE BERKELEY LABORATORY
UNIVERSITY OF CALIFORNIA
BERKELEY, CALIFORNIA 94720